Fabrication and heating rate study of microscopic surface electrode ion traps

2011 New J. Phys. 13 013032

(http://iopscience.iop.org/1367-2630/13/1/013032)

New Journal of Physics
The open-access journal for physics

Fabrication and heating rate study of microscopic surface electrode ion traps

N Daniilidis[1,2], S Narayanan[1,2], S A Möller[1,2], R Clark[2,3], T E Lee[4], P J Leek[5], A Wallraff[5], St Schulz[3], F Schmidt-Kaler[6] and H Häffner[1,7,8]

[1] Department of Physics, University of California, Berkeley, CA 94720, USA
[2] Institut für Quantenoptik and Quanteninformation, Innsbruck, Austria
[3] Center for Ultracold Atoms, Massachusetts Institute of Technology, Cambridge, MA, USA
[4] Department of Physics, California Institute of Technology, Pasadena, CA 91125, USA
[5] Department of Physics, ETH Zürich, CH-8093 Zürich, Switzerland
[6] Universität Mainz, QUANTUM, D-55128 Mainz, Germany
[7] Materials Sciences Division, Lawrence Berkeley National Laboratory, Berkeley, CA 94720, USA
E-mail: hhaeffner@berkeley.edu

New Journal of Physics **13** (2011) 013032 (17pp)
Received 15 September 2010
Published 24 January 2011
Online at http://www.njp.org/
doi:10.1088/1367-2630/13/1/013032

Abstract. We report heating rate measurements in a microfabricated gold-on-sapphire surface electrode ion trap with a trapping height of approximately 240 μm. Using the Doppler recooling method, we characterize the trap heating rates over an extended region of the trap. The noise spectral density of the trap falls in the range of noise spectra reported in ion traps at room temperature. We find that during the first months of operation, the heating rates increase by approximately one order of magnitude. The increase in heating rates is largest in the ion-loading region of the trap, providing a strong hint that surface contamination plays a major role for excessive heating rates. We discuss data found in the literature and the possible relation of anomalous heating to sources of noise and dissipation in other systems, namely impurity atoms adsorbed onto metal surfaces and amorphous dielectrics.

[8] Author to whom any correspondence should be addressed.

Contents

1. Introduction

Trapped ions provide a promising candidate for pursuing quantum information processing. Successful implementations of basic quantum protocols as well as the creation of entangled states support this view [1, 2]. A promising route to the scalability of ion-trap-based quantum information processing was proposed in which segmented trap electrodes allow splitting, shuttling and recombination of ion crystals [3, 4]. To overcome the difficulties of assembling three-dimensional (3D) trap structures and to simplify fabrication, several groups are developing planar (surface) ion traps where all electrodes lie within one plane and can be constructed using standard microfabrication methods [5]–[11]. In particular, recently the NIST group successfully transported ions through junctions in such planar traps [12].

Despite recent progress, there are still a number of unresolved difficulties with miniaturized traps. In an effort to develop this technology, one strives for miniaturization in order to easily achieve the high trap frequencies required for the fast splitting of ion crystals [5], and to increase coupling rates in approaches where trapped ions are coupled to [13] or via solid state elements [14]. Thus, planar traps with ion-surface separations of less than 100 μm are being pursued. However, the observed electric field noise is more than 3 orders of magnitude higher than that expected from Johnson noise considerations [3, 15], imposing a major obstacle in developing this approach.

This so-called anomalous heating in ion traps is usually discussed in terms of the patch potential model [16]. The essential features of this model are that the electric field noise responsible for heating the ion motion arises from a large number of randomly fluctuating sources and that the electric field of individual sources scales with source–ion separation as an electrical dipole field. These two features reproduce the observed $1/d^4$ scaling of the electric field noise with separation d between the ion and trap electrodes. Besides the scaling with distance, the noise spectral density of anomalous heating is believed to scale as $1/f$ with frequency [16] and experiments have indicated an increase in noise on particular traps with time, possibly due to contamination of the trap electrodes [16, 17]. More recently, it has been found that the noise is drastically reduced at low temperatures [9], and seems to be related to thermally activated processes [18], further supporting the $1/f$ nature.

This phenomenology suggests a connection with noise in various other systems. Electric field noise is a factor in nanomechanics [19], single spin detection [20] and

measurement of weak forces (e.g. gravitation) [21]. Moreover, charge noise limits the performance of nanoelectronic and quantum electronic devices, such as single electron transistors [22], Josephson qubits [23], superconducting coplanar resonators [24]–[26] and quantum dots [27, 28]. In these systems, decoherence is believed to be caused by tunneling two-level systems (TLSs), which possess a dipole moment [29, 30]. Such TLSs are common in amorphous dielectrics and are known to contribute to dielectric losses and the attenuation of phonons [31]–[33]. The latter mechanism has also been suggested to be relevant in dissipation encountered in efforts to laser cool dielectric mechanical resonators [34].

In a different direction, in measurements of non-contact friction using metalized atomic force microscope cantilevers close to metal surfaces, dissipation 9 to 11 orders of magnitude higher than expected for clean metal surfaces is observed [35]–[37], albeit at a different frequency and distance regime than those accessible with ion traps. This effect is suggested to be due to impurity atoms adsorbed onto the metal surfaces, and it is suggested that less than one atomic monolayer of adsorbate is sufficient to produce this effect [37]. In addition, the initially high level of dissipation close to metal surfaces has been found to further increase by up to two orders of magnitude upon deposition of dielectrics onto a gold surface [38].

Finally, magnetic traps for neutral atoms also suffer from electromagnetic field noise [39]. In this case, magnetic fields in the radio or microwave frequency range couple to the atomic spins and result in atom loss by causing spin flips. In contrast to the situations discussed above, this mechanism is well understood and accounted for by the Johnson noise on metallic trap electrodes [40].

Here, we study anomalous heating in ion traps. We describe a simple method for the fabrication of planar traps and measure their heating rates using the Doppler recooling method [41]. Taking advantage of the segmented trap geometry, we measure heating rates at various positions above the trap and find strong time and position dependence, which indicates a major role of surface contamination in excess heating rates. The heating rates in the ion-loading region of the trap have increased by more than one order of magnitude over the time span of a few months. In contrast, the heating rates sufficiently far from the loading region remain low throughout our study.

Finally, we present a phenomenological model for anomalous heating in ion traps that matches the above general context. This is done by adapting the patch potential model assuming a distribution of oscillating microscopic dipoles on the trap electrodes, with properties such that the $1/f$ nature of noise in ion traps is reproduced. Using this model, we estimate the density of electrical dipole sources on a trap electrode surface that would give rise to heating rates reported in the literature. In this context, we discuss the possible relevance of impurity atoms adsorbed onto trap electrodes and tunneling TLSs to anomalous heating in ion traps. Our model also explains why no 'anomalous' heating effects are observed in magnetic atom traps.

2. Experimental setup

We trap $^{40}Ca^{+}$ ions in an asymmetric surface electrode trap with a trapping height of approximately 240 μm, a schematic of which is shown in figure 1(a). A resistive oven produces a beam of neutral calcium atoms propagating parallel to the trap plane and along the axis of the trap. Great care is taken to minimize the direct exposure of trap surfaces to the atomic beam: a stainless-steel block, elevated by 200 μm above the plane of the trap, shields the trap from the calcium produced by the oven, as shown in figure 1(b). Measurements of fluorescence of neutral

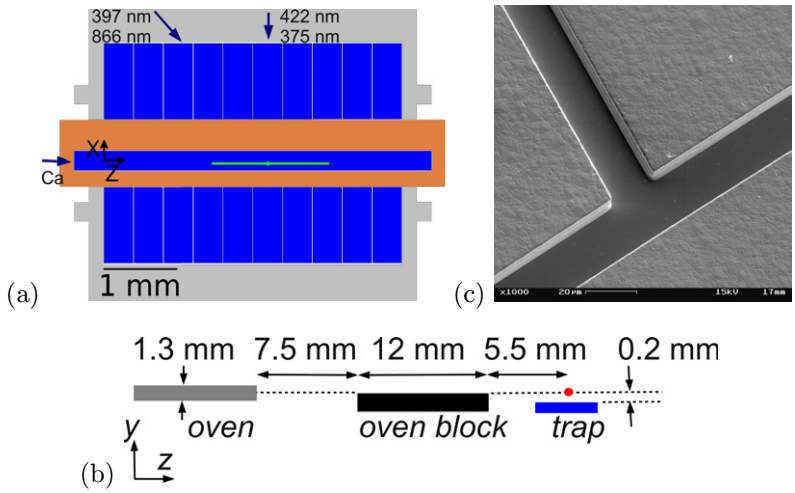

Figure 1. (a) Simplified schematic of the trap on which extensive measurements were made. Detail of the electrodes used for wire bonding to the electrodes on the periphery of the chip are not shown for simplicity. The ground electrode is shown in gray, the RF electrode in orange and the dc electrodes in blue. The gaps between electrodes in this trap are 10 μm wide. The green line along the z-axis on the central dc electrode indicates the range of axial positions in which the heating rates shown in figure 4 were measured. The circular mark on this line indicates the location used as a loading region, around which the highest increase in heating rates was observed. The arrows indicate the directions of laser beams and of the neutral Ca beam. The center of the coordinate system is indicated by the axes. (b) Side view of the trap-loading geometry, discussed in section 2. (c) Detail of the trap electrodes for a trap similar to the one for which heating rates were made. The electrode thickness is approximately 5 μm, and the gap between the electrodes in this case is 20 μm. The darker shade of the top surface of the trap is due to the presence of a thin layer of silver on the trap, deposited to reduce charging of the dielectric substrate in the SEM.

calcium produced by the oven beam reveal undetectably low fluorescence level at a height of 100 μm above the trap plane. The Ca atoms are photo-ionized in the trapping region with a two-photon process from the ground state to the continuum via the $4^1P_1^0$ state using 250 mW cm^{-2} of laser light at 422 nm (first stage) and 750 mW cm^{-2} at 375 nm (second stage). Both laser beams are focused to waists of approximately 100 μm.

The trap is driven at frequency $\Omega_{RF}/2\pi \approx 15$ MHz. This drive is amplified by a radio-frequency (RF) amplifier to approximately 100 mW and stepped up via a helical resonator in a quarter-wave configuration to a voltage of amplitude typically around 100 V. This is fed to the RF electrodes of the trap, with capacitance at the RF feedthrough of approximately 10 pF. The dc electrodes placed on either side of the RF electrodes are used to move the ion along the axial direction and to compensate micromotion [42]. The dc voltages used for trapping are between -10 and 15 V, resulting in trap frequencies of $(f_x, f_y, f_z) \approx (1.2, 1.4, 0.4)$ MHz in the horizontal radial, vertical radial and axial directions, respectively. When the Doppler cooling lasers are switched off, ions typically remain in the trap for between 5 and 30 s depending on whether a high or low heating rate region of the trap is used.

A diode laser stabilized at 794 nm is frequency doubled using a ring cavity to produce a wavelength of 397 nm, used for Doppler cooling and the detection of ions. A second diode laser at 866 nm acts as a repump. Both lasers are frequency stabilized to within 100 kHz with independent cavities using the Pound–Drever–Hall method. The frequencies of the lasers can be varied by changing the cavity lengths with piezoelectric elements and the 397 nm laser frequency can also be adjusted without affecting the cavity using an acousto-optic modulator in a double-pass configuration. The detection laser at 397 nm is intensity stabilized at the trap to a value of 38 mW cm^{-2}. The intensity of the 866 nm repump laser is adjusted at approximately 115 mW cm^{-2}.

Ion fluorescence is collected by a microscope objective with NA = 0.27. It is simultaneously detected by a photomultiplier tube and a CCD camera, using a 9 : 1 beam splitter. This configuration yields on the photomultiplier a maximum of 110 kcounts s^{-1}, which is reduced to 50 kcounts s^{-1} after the cooling laser powers have been adjusted.

3. Planar trap design

For our heating rate measurements, we use a planar trap with an asymmetric RF electrode. The ratio between the widths of the two RF rails is 2 : 1 (see figure 1). This geometry gives rise to a tilted RF quadrupole with a tilt angle with respect to the vertical (Y) direction of approximately 25°, which allows efficient laser cooling of both radial modes. In this configuration, standard Paul trap operation conditions can be achieved by aligning the static potential quadrupole with the RF quadrupole. Then ion motion along each of the trap axes is described by the usual Mathieu equations [43]. If the static and RF quadrupoles are not tilted by the same amount, the result is coupling of the Mathieu equations for ion motion in different directions. To see this more clearly, we note that one can express the axially invariant quadrupoles as $V_0\,(a\,(x^2 - y^2) + bxy)$. This can be expressed in the minimal form $V_0'\,(x'^2 - y'^2)$ in some tilted system of axes $X'Y'$. If the ratio a/b is not the same for the RF and static quadrupoles, then there exists no tilted system in which both potentials acquire the minimal form, and the Mathieu equations for the x- and y-directions are coupled. This will lead to coupling of the different modes of ion motion and could modify trap stability [44]. The situation will occur in all cases where the static and RF quadrupoles are not aligned with each other and can arise in both symmetric and asymmetric, as well as in 3D, linear traps.

The trap used in this work was designed with the goal of having several independent trapping regions on the same device. Thus, it has 10 pairs of dc electrode segments on each of the two outer sides of the RF electrodes (see figure 1). This gives enough freedom to trap in different regions of the trap and to transport ions along the trap axis. A central dc segment is located directly underneath the ion, facilitating micromotion compensation in the vertical direction [42]. The central segment is 250 μm wide, while the dc segments on the sides of the RF electrodes are 1000 μm by 400 μm in the X- and Z-directions, respectively. The widths of the RF electrodes are 400 and 200 μm, respectively.

4. Trap fabrication and preparation

We fabricated this design with a minimum dimension (gaps between trap electrodes) of 10 μm and electrode thickness of approximately 5 μm. The trap electrodes are deposited on a sapphire substrate, which has rms surface roughness of less than 1 nm. The initial step is evaporation

of a 5 nm-thick titanium adhesion layer, followed by evaporation of a 100 nm-thick gold layer. Evaporation of both is done uniformly on the substrate. Photolithography is carried out using a negative photoresist (micro resist technology, ma-N 440), suitable for deposition of resist with a thickness of several micrometers. After the development step (micro resist technology ma-D 332S), the photoresist is removed from the parts of the substrate where trap electrodes will be deposited and only the regions where the sapphire substrate will be exposed are covered by a photoresist of approximately 4.5 μm thickness.

The evaporated gold acts as a seed layer during electroplating using a commercial gold electroplating solution (Metalor, ECF 60) at a temperature of 50 °C and current density of 1.4 mA cm^{-2}. The resulting deposition rate is approximately 75 nm min^{-1} and the process is carried on for 70 min. The resulting gold layer has a thickness varying between 4.4 and 6.3 μm on different areas of a circular 50 mm-diameter wafer. The surface rms roughness of the gold film as measured with a surface profilometer is approximately 17 nm. After electroplating, the photoresist is removed and the seed layer is etched away using diluted 'aqua regia', with $HCl : HNO_3 : H_2O$ in a 3 : 1 : 7 ratio. In this process, etching of the seed layer in the regions of the gaps between trap electrodes will proceed at a rate considerably slower than in the rest of the trap, due to insufficient wetting of high-aspect-ratio troughs by the etching solution. To improve the etching rate of the seed layer, we use a surfactant (Triton X-100). Finally, after removal of the gold seed layer, a longer titanium-specific etching step to remove the remains of the titanium adhesion layer is performed in a diluted hydrochloric acid solution (32% HCl with addition of Triton-X 100, heated to 50 °C). The final etching steps do not influence the surface roughness of the trap electrodes. Before installation in vacuum, all traps are cleaned in a sequence of acetone/isopropyl alcohol/deionized water baths and blow dried in a nitrogen gas stream.

Using the above procedure, we have fabricated traps of various sizes. The ion trapping height in these varies between 500 and 125 μm. We successfully trapped single ions in three of those traps, the first with an ion height of 500 μm above the trap surface, and the other two with an ion height of approximately 240 μm. For what follows, we focus on one of the latter, which was studied extensively. Prior to the heating rate measurements, this trap was baked in vacuum at 150 °C for two weeks, to reach a base pressure of 2×10^{-10} mbar.

5. Heating rate measurement method

The heating rates of the trap were measured using the Doppler recooling method in which the motional energy of the ion is determined by taking advantage of the increased Doppler shift for an ion with increased kinetic energy [41]. This allows one to estimate the ion energy by comparing the instantaneous ion fluorescence to the steady-state fluorescence level of a Doppler-cooled ion. To evaluate the change in fluorescence, Doppler cooling of the ion is turned off for time τ_{off} during which time the ions heat up. The change in the ion fluorescence is monitored as the ion cools down after turning the Doppler cooling on. This change in fluorescence level is used to determine the energy that the ion acquired during τ_{off} and thus deduce the ion heating rate.

Application of the Doppler recooling method, as described in the original proposal, is practical for situations where the ion mode that is Doppler cooled does not experience significant micromotion, for example, to cooling of the axial mode of a linear Paul trap. While this geometry is frequently sufficient, it is not applicable whenever a single Doppler cooling beam is available, as in situations where planar traps are part of a complex setup granting limited

optical access to the ions. In these cases micromotion contribution to Doppler broadening can be significant and has to be taken into account in determining ion energy from changes in fluorescence. Following the procedure discussed in [41], we numerically find that for our experimental parameters, micromotion contributes significantly to Doppler broadening, and can lead to an overestimation of the ion energy by a factor between 2 and 4 if the method is applied without accounting for micromotion. Nevertheless, the numerical integration required to obtain and fit fluorescence recooling curves to experimental data is computationally intense, which makes it cumbersome.

In the case of $^{40}Ca^{+}$ ions, further complications to the application of the Doppler recooling method arise due to the electronic level scheme, which is more complicated than that of a simple two-level atom. In order to estimate the ion energy, the linewidth of the resonance and the saturation parameter(s) are required. For a two-level ion, this is straightforward; however, for multi-level dynamics, the situation is more complex. In particular, dark resonances and the strength of the repump light field(s) have significant influence on the line shape [45]–[47].

One possible resolution is the detailed modeling of the dynamics and careful measurement of all relevant laser parameters, such as detunings and intensities. Nevertheless, due to the complexity of the situation, instead of modeling the recooling dynamics in the presence of micromotion and multiple atomic levels, we use here a simple workaround by calibrating the energy scale with well-defined electric field noise. Apart from ease of implementation, a further advantage is that one can separate out the effect of different energies of the three motional modes on the fluorescence signal by choosing particular noise frequency bands and/or excitation geometries, i.e. the electrodes to which the noise is applied. Thus, one can study or avoid implicit assumptions while extracting a single heating rate for the three motional modes.

For these experiments, the intensity of the laser beam that we use for laser cooling and detection at 397 nm is actively stabilized at a value of 38 mW cm^{-2}. The frequency of this laser is detuned to 5 MHz on the red side of the resonance of $S_{1/2} \leftrightarrow P_{1/2}$. This choice of detuning provides better sensitivity for the recooling measurements compared to the optimal detuning of 10 MHz normally used for the Doppler cooling of $^{40}Ca^{+}$. The intensity of the 866 nm repump laser is adjusted at 115 mW cm^{-2}, and its frequency is adjusted to the $P_{1/2} \leftrightarrow D_{3/2}$ transition by maximizing the fluorescence level. To measure recooling curves, we turn off Doppler cooling and allow the ion to heat by switching off the repump laser at 866 nm for time τ_{off}. During a time interval $t_{\mathrm{pump}} \sim 0.1\,\mu\mathrm{s} \ll \tau_{\mathrm{off}}$, the ion gets pumped into the $D_{3/2}$ level and will not be cooled by the Doppler cooling laser. After the repump laser is turned on, ion fluorescence is acquired using time bins of 50 μs. The procedure is repeated typically 1000 times and the fluorescence curves are averaged to improve the statistics. The inset in figure 2 shows a typical recooling curve obtained using this procedure.

To extract the ion energy from the recooling curves, we use the analysis procedure of [41]. The recooling fluorescence curves are fitted assuming a 1D harmonic oscillator having a projection along the laser beam equal to the smallest projection of the three ion modes. We thus extract a quantity ϵ, to which we will refer as the scaled energy. This would correspond to an effective average energy of the three modes of the ion in the case of a two-level ion experiencing no micromotion, but in our case it is found to be merely proportional to the ion energy. This is evident in the linear increase in ϵ with heating time τ_{off}, as shown in figure 2.

To calibrate the scaled energy, we heat the ion with externally supplied electric field noise provided by a signal generator that has been calibrated against a spectrum analyzer. The noise is white to a very large degree, with spectral density at the ion secular frequencies varying by less

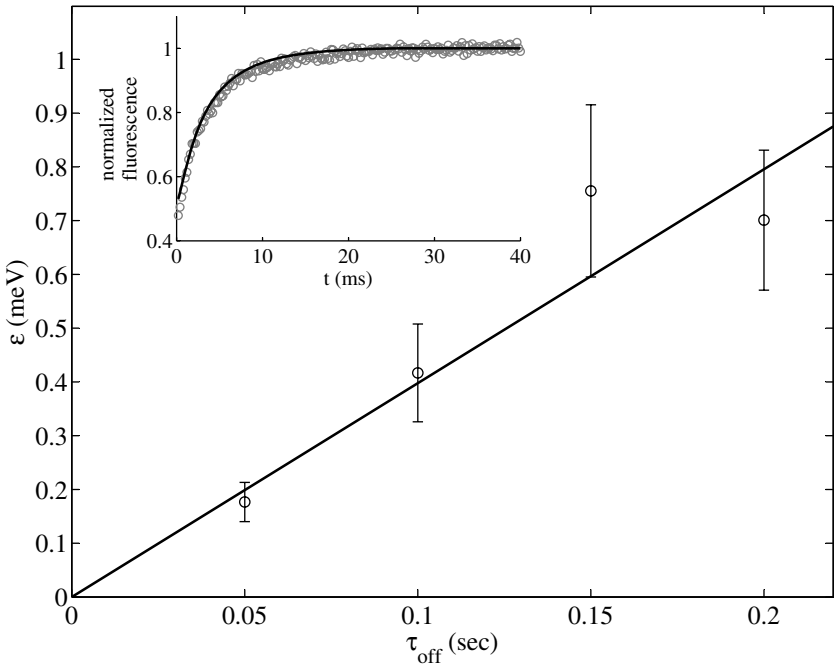

Figure 2. Scaled energy ϵ as a function of ion heating time τ_{off} in Doppler recooling experiments. As expected, the energy of the ion scales linearly with heating time and a linear fit constrained through the origin is used to derive the rate of change $\mathrm{d}\epsilon/\mathrm{d}t$, in this case $4.0 \pm 0.3\,\text{meV}\,\text{s}^{-1}$. Uncertainties in the ion energy are determined by uncertainty in the exact value of the detuning used for the measurement. Inset: a typical Doppler recooling curve for one value of τ_{off} with fluorescence as a function of time, and fitted (solid line) according to the procedure described in [41]. Time zero in the inset corresponds to the onset of recooling, i.e. turning on the repump laser at 866 nm.

than 10%. We vary the noise spectral density between 4.4×10^{-16} and $2.5 \times 10^{-14}\,\text{V}^2\,\text{Hz}^{-1}$. The noise is applied to one of the trap electrodes with almost equal projection of the electric field on all three modes of ion motion and the corresponding electric field noise at the ion position is changed between 1.7×10^{-11} and $1.0 \times 10^{-9}\,(\text{V m})^{-2}\,\text{Hz}^{-1}$.

The calibration is performed by determining the heating rate $\mathrm{d}\epsilon/\mathrm{d}t$ from the recooling curves and comparing it to the expected ion heating rate $\mathrm{d}E/\mathrm{d}t$, at various levels of applied external noise. The latter is calculated using [16]

$$E = \sum_{i=\{x,y,z\}} \frac{e^2}{4m} S_{\text{E}}(\omega_{\text{i}})\,\tau_{\text{off}}, \tag{1}$$

where τ_{off} is the time during which the ion is allowed to heat before measuring its energy, ω_i is the secular frequency of the i^{th} mode of the ion and $S_{\text{E}}(\omega_{\text{i}})$ is the power spectral density of the electric field at that frequency. In this expression, heating of the secular sidebands of the micromotion at $\Omega_{\text{RF}} \pm \omega_{\text{i}}$ is omitted, since it is expected to be weaker by a factor of $(\omega_{\text{i}}/\,\Omega_{\text{RF}})^2 \sim 0.01$, which is significantly below the accuracy of this method.

Heating rates are determined for different values of the externally applied noise. The results of such measurements are shown in figure 3, where we plot $\mathrm{d}\epsilon/\mathrm{d}t$ versus $\mathrm{d}E/\mathrm{d}t$. We find

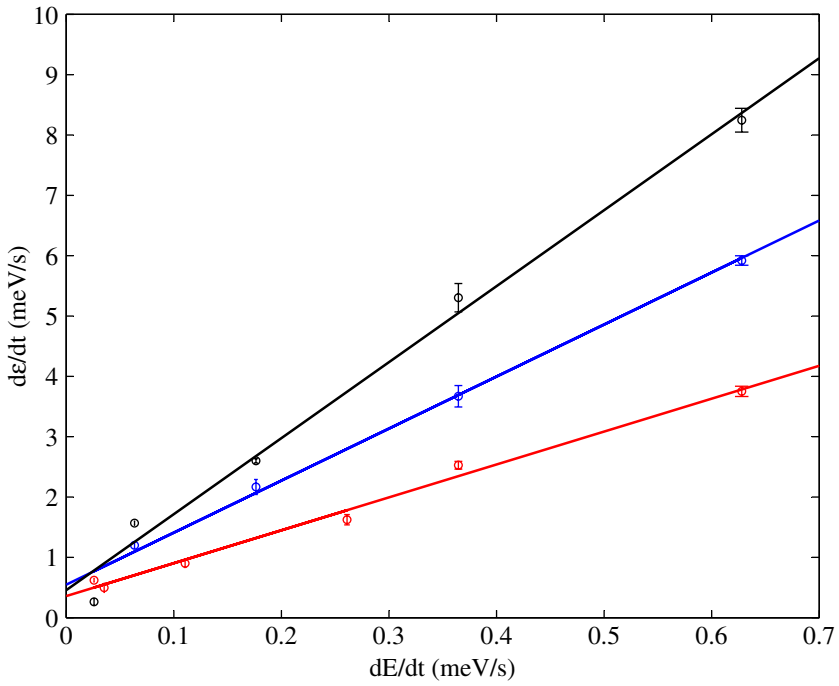

Figure 3. Calibration of the scaled energy, ϵ, determined from recooling curves against the externally applied noise source. Shown is $\mathrm{d}\epsilon/\mathrm{d}t$, determined from the procedure outlined in the text and in figure 2, versus the externally induced heating rate $\mathrm{d}E/\mathrm{d}t$, determined from equation (1), for different magnitudes of applied noise. Also shown are linear fits to the data. Different curves were measured with a minimum separation of 4 h.

linear dependence on time scales of about 1 h, but the slopes between different trends taken several hours apart vary by up to a factor of roughly 2. This is most likely due to drifts in the experimental parameters that we do not stabilize accurately, namely the repump laser detuning and intensity. From linear fits to these curves, we determine ϵ to be a factor of 8.9 ± 3.6 higher than the actual energy acquired by the ion. As a result, the uncertainty in our determination of heating rates of our trap is ultimately determined by the uncertainty in the calibration of ϵ versus E. We note that this calibration method provides information about the electric field amplitude noise, which determines the energy acquired by all three modes of the ion. This is in contrast to the application of the Doppler recooling method, when the laser beam is parallel to one of the main trap axes, and the sideband cooling method, where the electric field noise along only one mode is probed.

6. Results and discussion

Heating rate measurements were performed at different positions along the axis of the trap, as shown in figure 4. The measured results have been normalized to phonons of 1 MHz frequency. The single filled data point at axial position of 2250 μm was measured one-and-a-half months after the installation of the trap in vacuum and the open data points were obtained later, after an abrupt increase in heating rates of our trap. This occurred after approximately two months of

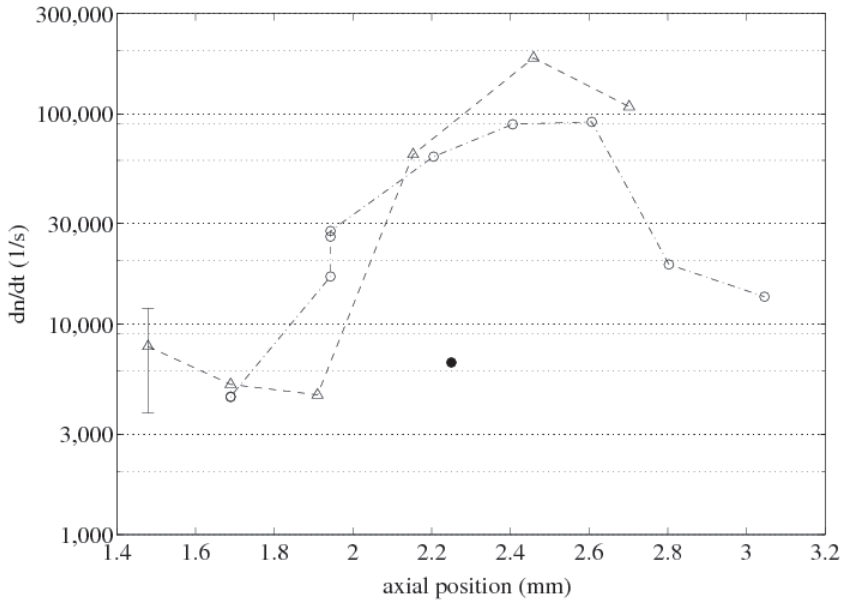

Figure 4. Heating rate, normalized to 1 MHz phonons, at different positions along the axis of the trap and at different times. The total number of phonons of all three modes is shown. A representative errorbar is shown on the data point at position 1.5 mm. The filled data point at 2.25 mm was measured in the 'pristine' trap, i.e. after one-and-a-half months of operation in vacuum. We mark the measurements performed 8 and 10 months after the initial installation of the trap in vacuum with the open black triangles and open black circles, respectively. At the time of the latter measurements, the heating rate around the ion-loading region had increased by one order of magnitude, as discussed in the text.

trap operation. It coincided with a failure of the ion pump used to maintain the ultrahigh vacuum and was followed by an increase in the stray electrostatic fields at the ion positions [42]. During the pump failure, elevated pressures of 10^{-7} mbar were reached in the vacuum chamber, whereas before and after the pressure was in the low 10^{-10} mbar range.

The heating rate appears to have a maximum around the region used for ion loading in the trap. This is the range of axial positions between roughly 1900 and 2700 μm, which was used extensively as an ion-loading zone. Far from the loading region the heating rate is close to the values measured in the 'pristine' trap one-and-a-half months after trap installation in vacuum. The heating rates near the loading zone of the trap increased from $\approx$5 phonons ms^{-1} to more than $\approx$50 phonons ms^{-1} in the first few months of trap operation. Far from this zone, the heating rates maintained their lower value. Likewise, uncooled ion lifetimes decreased by roughly one order of magnitude in the parts of the trap where increased heating rates were observed.

The change in heating rates coincided with an abrupt increase in stray static fields in the same region of the trap [42] and it is very likely that both of these effects are related to extensive use of the region around the axial coordinate of 2250 μm as a loading zone. A number of effects can be responsible for the change in trap behavior. From the geometry of our vacuum apparatus, we expect that possible Ti contamination from the titanium sublimation pump is rather homogeneous. Similarly, surface contamination with atomic Ca from the oven is not

expected to peak at the loading zone, located near the center of the trap, but rather to fall off monotonically moving towards the oven direction as a result of the atomic beam flux screening, as discussed in section 2. One possible mechanism of surface contamination is the bombardment of the trap electrodes by electrons created during trap loading or by $^{40}Ca^{+}$ ions, which are created by photoionization outside the trapping volume. These can impinge on the gold surface with energies of up to 100 eV when accelerated by the RF field. $^{40}Ca^{+}$ ions with energies of a few eV can get physisorbed onto the trap electrodes and later form chemical compounds, while ions at higher energies can sputter material from the trap surface. In addition, it is possible that the laser light used for ion creation and detection locally alters the chemical composition.

As the mechanism leading to heating of trapped ions is not fully understood, it is useful to summarize heating rates in different traps constructed from different electrode materials and used to trap different ion species. Since the noise spectral density, $S_{\mathrm{E}}(\omega)$, causing anomalous heating is believed to scale as $1/f$ with frequency [16], it is convenient to regularize experimental results by deriving $\omega_{\mathrm{i}}\, S_{\mathrm{E}}(\omega_i)$ [48], where ω_{i} is the frequency of the ion mode that is being measured. This is straightforwardly done for heating rate measurements performed using the sideband spectroscopy method, where the heating rate of a specific secular mode can be measured. In order to regularize results measured using the Doppler recooling method, one needs to take into account that the energy of all three secular modes is redistributed and finally removed from the ion, as discussed in [41]. Thus, a properly averaged 'effective' frequency has to be used. By energy conservation considerations, and assuming for simplicity that the electric field noise is isotropic, we find that the effective frequency is $\bar{\omega}^{-1} = \sum_{i=1}^{3} \omega_{\mathrm{i}}^{-1}$. In our measurements, the axial frequency is significantly smaller than the radial ones and $\bar{\omega}$ turns out to be very close to the axial frequency.

Using this approach, we have compiled a graph of representative data found in the literature [6, 9, 11], [15]–[18], [48]–[56] (see figure 5). In the graph, we specify ion species used in the measurements and trap electrode material, as well as the temperature of the trap, if other than room temperature. We include some of the measurements performed in cooled trap apparatuses, but focus on the room-temperature results where measurements are abundant. We observe that the majority of traps measured at the same temperature fall around a general trend following a d^{-4} law (corresponding to the diagonal of the figure). The traps with the lowest heating rates are a molybdenum ring trap [16] used to trap $^{9}Be^{+}$ and a gold-on-quartz surface trap [48] used to trap $^{25}Mg^{+}$. Nevertheless, the presence of both gold and molybdenum traps with noise spectral densities well within the average implies that more than material specific the source of the noise is specific to trap preparation and cleaning procedures. As we discuss in what follows, less than one monolayer of adsorbed impurity atoms, as well as a thin dielectric layer formed on the trap surface, can be responsible for the observed heating rates.

7. Model for anomalous heating

We now proceed to derive a phenomenological model for electric field noise above metal surfaces that can provide physical information about the possible sources of anomalous heating in ion traps. We build on the insight provided by the patch potential model: the electric field of individual noise sources scales as an electric dipole field, thus reproducing the correct scaling of noise spectral density with ion-trap distance. In discussions about the patch potential model, the noise source is not considered in detail but is generally thought to be related to the polycrystalline structure of the metal electrodes [16, 57]. Here, we consider a different noise

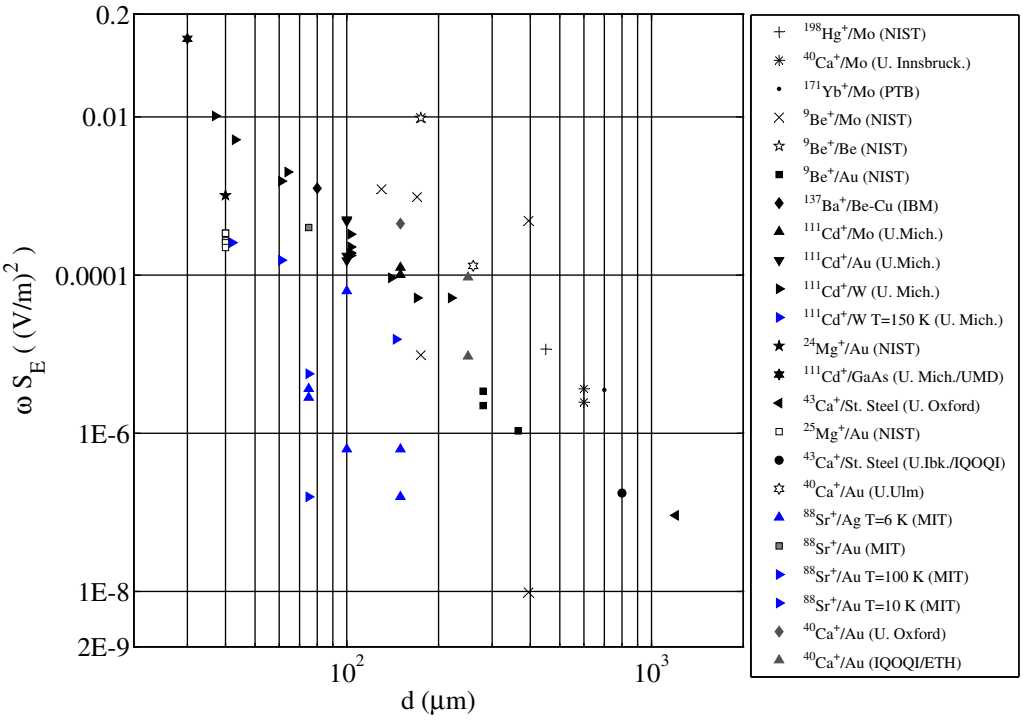

Figure 5. Summary of representative noise spectral densities for different traps found in the literature, plotted versus ion-trap distance d. We plot electric field noise in only one component of the electric field. The ion species and trap electrode material are specified. The temperature is specified when different than room temperature. The references are organized in chronological order of appearance. The trap used in this work fell well within the average trend initially (lower point, corresponding to heating rate measured 1.5 months after installing the trap in vacuum), but still falls within the limits of the trend even after deterioration of trap performance. The diagonal in the figure corresponds to a d^{-4} trend. Data are from [6, 9, 11], [15]–[18], [48]–[56].

source by assuming the sources to be electrical dipoles that can form on metal surfaces, even in ultrahigh vacuum conditions. In addition, we introduce to the dipole sources the required spectral features to reproduce the scaling of noise spectral density with frequency. These assumptions allow us to relate the magnitude of the observed noise to physical properties of the noise sources. Finally, in order to help to identify possible noise sources, we provide some estimates that incorporate the developments in other fields, as already mentioned in section 1.

In many situations, $1/f$ noise is attributed to systems with a Debye-type relaxation and a distribution of relaxation rates [58]. Accordingly, we consider a typical dipole with dipole moment μ and relaxation rate Γ, leading to an autocorrelation function

$$\phi_\mu(t) = \mu^2 \, \mathrm{e}^{-\Gamma t}. \tag{2}$$

The corresponding dipole spectral density is

$$S_\mu^\Gamma(f) = \frac{2\mu^2\Gamma}{\Gamma^2 + (2\pi f)^2}. \tag{3}$$

To recover the $1/f$ noise spectrum, we assume a distribution of relaxation rates scaling as $F(\Gamma) = A/\Gamma$, where the normalization $A = \ln(\frac{\Gamma_{\max}}{\Gamma_{\min}})$ depends only logarithmically on the limiting relaxation rates. In the context of thermally activated dipole relaxation, A corresponds to the range of energy barriers through which relaxation can occur. The dipole moment spectral density is now obtained,

$$S_\mu(f) = \frac{A\mu^2}{2f}. \tag{4}$$

Fluctuating dipoles on the trap electrodes produce at the ion position, a distance r away, a fluctuating electric field with components, in some direction i, of order $E_i = \frac{\mu}{2\pi\epsilon_0 r^3}$. This relation will not be exact: the components of the electric field in directions parallel and perpendicular to the surface will differ, a fluctuating dipole near a conducting surface will get either enhanced or screened depending on its orientation [59] and the exact mechanism of screening of charges by metal surfaces at separations of the order of interatomic distances is unclear [60]. Nevertheless, this value will suffice for our current estimates. Moreover, fluctuating electric dipoles will produce negligible magnetic field noise. The reason is that in the near field of dipole radiation, the electromagnetic field is predominantly electric. The near-field condition is always satisfied in current experiments, and so this mechanism will cause electric field noise and virtually no magnetic field noise.

To estimate the electric field noise spectral density, we perform statistical averaging that results in scaling as $\sqrt{N}$ with the number, N, of dipoles. The noise spectral density from a planar trap with surface density n_S of dipoles is then given by the integral over the trap surface,

$$S_E(f) = n_s \int_{\text{surf}} \left(\frac{1}{2\pi\epsilon_0 r}\right)^2 S_\mu(f)\, d\alpha = \frac{A n_S \mu^2}{8\pi\epsilon_0^2 d^4 f}. \tag{5}$$

The rudimentary result of equation (5) allows us to estimate the product $n_S\,\mu^2$ of the density of dipoles on the trap surface with the squared dipole moment, based on the measured noise spectral density, secular frequency and ion-trap distance. We use this result to evaluate different possible sources of anomalous heating due to contaminated trap electrode surfaces. By assuming a typical dipole moment of 1D and value of normalization constant $A \approx 10$ as reasonable estimates, the value of the average trend of heating rate data in figure 5 leads to $n_S \approx 6 \times 10^{19}\,\text{m}^{-2}$. This value corresponds to typical surface densities of atoms on solid surfaces.

First, we consider impurity atoms adsorbed onto the trap electrodes, following the analysis of Volokitin and Persson [37]. In this case, a metal surface with small coverage by adsorbed molecules can give rise to dissipation and noise several orders of magnitude higher than those expected from a clean metal surface. To put this into the context of our model, we consider adsorbed atoms on the metal surface, which form polar bonds and can switch between different configurations giving rise to fluctuating dipoles. As a typical dipole moment, we take the value for Cs adsorbed on Cu(100) as considered in [37], i.e. $\mu \approx 4$D. Using equation (5), we obtain a coverage fraction $\theta \approx 0.6$ for a disordered gold surface, which is a very reasonable result. While in the case of tunneling TLSs, which we consider next, the typical ranges of activation energies and relaxation times are somewhat known and well understood, such details are in general unclear for surface adsorbates. Nevertheless, this mechanism requires less than one monolayer of adsorbate and can, as a result, be very common unless specific care is taken to target and remove material-specific adsorbates from metal surfaces.

We also consider tunneling TLSs in an amorphous dielectric film on the trap electrodes as the fluctuating dipoles. The thickness of the dielectric layer can be estimated as $\delta = n_S/n_V$, where n_V is the density of TLSs in the dielectric. When this quantity is relatively well determined at temperatures in the few K range [33], the situation at higher temperatures is unclear. It has been argued that the TLS density of states increases linearly with temperature [61], and according to that estimate one obtains at room temperature a density $n_V \approx 5 \times 10^{27}\,\mathrm{m}^{-3}$ of TLSs with energies less than the estimated upper limit of 0.1 eV [31, 32]. With the above value of n_s, this would correspond to a dielectric of thickness $\delta \approx 10\,\mathrm{nm}$. While this is a high value, it is only intended as an order of magnitude estimate, given the crudeness of the approximations used. It is possible that oxides on metal surfaces, residues of fabrication, gases adsorbed onto the trap electrodes and material are deposited on trap surfaces while the trap is in operation form dielectric layers in the nanometer range.

8. Summary and conclusions

We have reported a simple fabrication method for segmented planar ion traps, suitable for ion transport and for operation with a tilt of the main trap axes with respect to the direction perpendicular to the trap plane. We have described a modification of the Doppler recooling method for heating rate measurements and used the method to measure heating rates of one gold-on-sapphire planar trap. The heating rates were found to deteriorate with time, and to be position dependent with a maximum around the loading zone of the trap, suggesting surface contamination as a major source of anomalous heating. We have presented a phenomenological model that can explain anomalous heating in ion traps and used it to evaluate different possible sources of anomalous heating encountered in other systems. We found that both adsorbed impurity atoms close to a density of one monolayer and tunneling TLSs in amorphous dielectrics on the trap electrodes can be responsible for the observed heating. Careful surface characterization and cleaning procedures of ion traps are needed to reach a more definite conclusion about the sources of and solutions to anomalous heating.

Acknowledgments

We thank John Martinis and Gabor A Somorjai for useful discussions, and D Frank Ogletree for pointing out important work on non-contact friction. This work was supported by the Austrian Ministry of Sciences with a START grant. ND was supported in part by the European Union with a Marie Curie fellowship. SN was partially supported by the Laboratory Directed Research and Development Program of Lawrence Berkeley National Laboratory under the US Department of Energy contract no. DE-AC02-05CH11231 and SS was supported by the Alexander von Humboldt Foundation with a Feodor Lynen Fellowship. FSK acknowledges support by the European Commission with AQUTE and by the German-Israel Science Foundation.

References

[1] Häffner H, Roos C F and Blatt R 2008 Quantum computing with trap ions *Phys. Rep.* **469** 155
[2] Blatt R and Wineland D 2008 Entangled states of trapped atomic ions *Nature* **453** 1008–15
[3] Wineland D J, Monroe C, Itano W M, Leibfried D, King B E and Meekhof D M 1998 Experimental issues in coherent quantum-state manipulation of trapped atomic ions *J. Res. Natl Inst. Stand. Technol.* **103** 259–328

[4] Kielpinski D, Monroe C and Wineland D J 2002 Architecture for a large-scale ion-trap quantum computer *Nature* **417** 709–11
[5] Chiaverini J, Blakestad R B, Britton J, Jost J D, Langer C, Leibfried D, Ozeri R and Wineland D J 2005 Surface-electrode architecture for ion-trap quantum information processing *Quantum Inf. Comput.* **5** 419–39
[6] Seidelin S *et al* 2006 Microfabricated surface-electrode ion trap for scalable quantum information processing *Phys. Rev. Lett.* **96** 253003
[7] Britton J *et al* 2006 A microfabricated surface-electrode ion trap in silicon arXiv:quant-ph/0605170
[8] Pearson C E, Leibrandt D R, Bakr W S, Mallard W J, Brown K R and Chuang I L 2006 Experimental investigation of planar ion traps *Phys. Rev.* A **73** 32307
[9] Labaziewicz J, Ge Y, Antohi P, Leibrandt D, Brown K R and Chuang I L 2008 Suppression of heating rates in cryogenic surface-electrode ion traps *Phys. Rev. Lett.* **100** 13001
[10] Leibrandt D R *et al* 2009 Demonstration of a scalable, multiplexed ion trap for quantum information processing arXiv:0904.2599v1 [quant-ph]
[11] Allcock D T C, Sherman J A, Curtis M J, Imreh G, Burrell A H, Szwer D J, Stacey D N, Steane A M and Lucas D M 2009 Implementation of a symmetric surface electrode ion trap with field compensation using a modulated Raman effect arXiv:0909.3272v2
[12] Amini J M, Uys H, Wesenberg J H, Seidelin S, Britton J, Bollinger J J, Leibfried D, Ospelkaus C, VanDevender A P and Wineland D J 2009 Scalable ion traps for quantum information processing arXiv:0812.3907v1
[13] Tian L, Rabl P, Blatt R and Zoller P 2004 Interfacing quantum-optical and solid-state qubits *Phys. Rev. Lett.* **92** 247902
[14] Daniilidis N, Lee T, Clark R, Narayanan S and Häffner H 2009 Wiring up trapped ions to study aspects of quantum information *J. Phys. B: At. Mol. Opt. Phys.* **42** 154012
[15] Monroe C, Meekhof D M, King B E, Itano W M and Wineland D J 1995 Demonstration of a fundamental quantum logic gate *Phys. Rev. Lett.* **75** 4714–7
[16] Turchette Q A *et al* 2000 Heating of trapped ions from the quantum ground state *Phys. Rev.* A **61** 63418
[17] DeVoe R and Kurtsiefer C 2002 Experimental study of anomalous heating and trap instabilities in a microscopic ^{137}Ba ion trap *Phys. Rev.* A **65** 1–8
[18] Labaziewicz J, Ge Y, Leibrandt D, Wang S X, Shewmon R and Chuang I L 2008 Temperature dependence of electric field noise above gold surfaces *Phys. Rev. Lett.* **101** 180602
[19] Li M, Tang H X and Roukes M L 2007 Ultra-sensitive NEMS-based cantilevers for sensing, scanned probe and very high-frequency applications *Nat. Nanotechnol.* **2** 114–20
[20] Mamin H J, Budakian R, Chui B W and Rugar D 2003 Detection and manipulation of statistical polarization in small spin ensembles *Phys. Rev. Lett.* **91** 207604
[21] Speake C C and Trenkel C 2003 Forces between conducting surfaces due to spatial variations of surface potential *Phys. Rev. Lett.* **90** 160403
[22] Zimmerli G, Eiles T M, Kautz R L and Martinis J M 1992 Noise in the Coulomb blockade electrometer *Appl. Phys. Lett.* **61** 237–9
[23] Astafiev O, Yu Pashkin A, Nakamura Y, Yamamoto T and Tsai J S 2004 Quantum noise in the Josephson charge qubit *Phys. Rev. Lett.* **93** 267007
[24] Gao J, Daal M, Vayonakis A, Kumar S, Zmuidzinas J, Sadoulet B, Benjamin A M, Day P K and Leduc H G 2008 Experimental evidence for a surface distribution of two-level systems in superconducting lithographed microwave resonators *Appl. Phys. Lett.* **92** 152505
[25] Kumar S, Gao J, Zmuidzinas J, Mazin B A, LeDuc H G and Day P K 2008 Temperature dependence of the frequency and noise of superconducting coplanar waveguide resonators *Appl. Phys. Lett.* **92** 123503
[26] Aaron Connell D O *et al* 2008 Microwave dielectric loss at single photon energies and millikelvin temperatures *Appl. Phys. Lett.* **92** 112903
[27] Hayashi T, Fujisawa T, Cheong H, Jeong Y and Hirayama Y 2003 Coherent manipulation of electronic states in a double quantum dot *Phys. Rev. Lett.* **91** 1–4

[28] Gorman J, Hasko D and Williams D 2005 Charge-qubit operation of an isolated double quantum dot *Phys. Rev. Lett.* **95** 1–4
[29] Shnirman A, Schön G, Martin I and Makhlin Y 2005 Low- and high-frequency noise from coherent two-level systems *Phys. Rev. Lett.* **94** 1–4
[30] Martinis J 2005 Decoherence in Josephson qubits from dielectric loss *Phys. Rev. Lett.* **95** 1–4
[31] Anderson P W, Halperin B I and Varma C M 1972 Anomalous low-temperature thermal properties of glasses and spin glasses *Phil. Mag.* **25** 1–9
[32] Phillips W A 1972 Tunneling states in amorphous solids *J. Low Temp. Phys.* **7** 351–60
[33] Phillips W A 1987 Two-level states in glasses *Rep. Prog. Phys.* **50** 1657
[34] Arcizet O, Rivière R, Schliesser A, Anetsberger G and Kippenberg T 2009 Cryogenic properties of optomechanical silica microcavities *Phys. Rev.* A **80** 1–4
[35] Dorofeyev I, Fuchs H, Wenning G and Gotsmann B 1999 Brownian motion of microscopic solids under the action of fluctuating electromagnetic fields *Phys. Rev. Lett.* **83** 2402–5
[36] Persson B N J and Volokitin A I 2000 Comment on Brownian motion of microscopic solids under the action of fluctuating electromagnetic fields *Phys. Rev. Lett.* **2402** 3504–4
[37] Volokitin A I and Persson B N J 2005 Adsorbate-induced enhancement of electrostatic noncontact friction *Phys. Rev. Lett.* **94** 86104
[38] Kuehn S, Loring R and Marohn J 2006 Dielectric fluctuations and the origins of noncontact friction *Phys. Rev. Lett.* **96** 1–4
[39] Jones M, Vale C, Sahagun D, Hall B and Hinds E 2003 Spin coupling between cold atoms and the thermal fluctuations of a metal surface *Phys. Rev. Lett.* **91** 1–4
[40] Henkel C, Pötting S and Wilkens M 1999 Loss and heating of particles in small and noisy traps *Appl. Phys. B: Lasers Opt.* **69** 379–87
[41] Wesenberg J H *et al* 2007 Fluorescence during doppler cooling of a single trapped atom *Phys. Rev.* A **76** 53416
[42] Narayanan S, Daniilidis N, Moeller S, Clark R, Ziesel F, Singer K, Schmidt-Kater F and Haeffner H 2011 Electric field compensation and sensing using planar ion traps, in preparation
[43] Leibfried D, Blatt R, Monroe C and Wineland D 2003 Quantum dynamics of single trapped ions *Rev. Mod. Phys.* **75** 281324
[44] Shaikh F and Ozakin A 2010 Ion motion stability in asymmetric surface electrode ion traps *2010 DAMOP Meeting Houston, Texas, 61*
[45] Lindberg M and Javanainen J 1986 Temperature of a laser-cooled trapped three-level ion *J. Opt. Soc. Am.* B **3** 1008
[46] Siemers I, Schubert M, Blatt R, Neuhauser W and Toschek P E 1992 The 'Trapped State' of a trapped ion-line shifts and shape *Europhys. Lett.* **18** 139–144
[47] Reiss D, Lindner A and Blatt R 1996 Cooling of trapped multilevel ions: a numerical analysis *Phys. Rev.* A **54** 5133–40
[48] Epstein R J *et al* 2007 Simplified motional heating rate measurements of trapped ions *Phys. Rev.* A **76** 33411
[49] Diedrich F, Bergquist J C, Itano W M and Wineland D J 1989 Laser cooling to the zero-point energy of motion *Phys. Rev. Lett.* **62** 403–6
[50] Roos Ch, Zeiger Th, Rohde H, Nägerl H C, Eschner J, Leibfried D, Schmidt-Kaler F and Blatt R 1999 Quantum state engineering on an optical transition and decoherence in a Paul trap *Phys. Rev. Lett.* **83** 4713
[51] Tamm Ch, Engelke D and Bühner V 2000 Spectroscopy of the electric-quadrupole transition $^2S_{1/2}(F = 0)^2D_{3/2}(F = 2)$ in trapped $^{171}Yb^+$ *Phys. Rev.* A **61** 053405
[52] Deslauriers L, Haljan P C, Lee P J, Brickman K-A, Blinov B B, Madsen M J and Monroe C 2004 Zero-point cooling and low heating of trapped $^{111}Cd^+$ ions *Phys. Rev.* A **70** 43408
[53] Deslauriers L, Olmschenk S, Stick D, Hensinger W K, Sterk J and Monroe C 2006 Scaling and suppression of anomalous heating in ion traps *Phys. Rev. Lett.* **97** 103007

[54] Stick D, Hensinger W K, Olmschenk S, Madsen M J, Schwab K and Monroe C 2006 Ion trap in a semiconductor chip *Nat. Phys.* **2** 36
[55] Lucas D M, Keitch B C, Home J P, Imreh G, McDonnell M J, Stacey D N, Szwer D J and Steane A M 2007 A long-lived memory qubit on a low-decoherence quantum bus arXiv: 0710.4421v1
[56] Schulz S A, Poschinger U, Ziesel F and Schmidt-Kaler F 2008 Sideband cooling and coherent dynamics in a microchip multi-segmented ion trap *New J. Phys.* **10** 045007
[57] Dubessy R, Coudreau T and Guidoni L 2009 Electric field noise above surfaces: a model for heating-rate scaling law in ion traps *Phys. Rev.* A **80** 031402
[58] Dutta P and Horn P M 1981 Low-frequency fluctuations in solids: $1/f$ noise *Rev. Mod. Phys.* **53** 497–516
[59] Sommerfeld A 1949 *Partial Differential Equations in Physics* (New York: Academic)
[60] Feibelman P 1982 Surface electromagnetic fields *Prog. Surf. Sci.* **12** 287–407
[61] Varma C M, Dynes R C and Banavar J R 1982 Thermally created tunnelling states in glasses *J. Phys. C: Solid State Phys.* **15** L1221